



Mesoscale models for concrete: Homogenisation and damage behaviour

P. Wriggers*, S.O. Moftah

Institute for Mechanics and Computational Mechanics, University of Hannover, Hannover, Germany

Received 27 October 2005; received in revised form 27 October 2005; accepted 20 November 2005
Available online 9 January 2006

Abstract

In this paper three-dimensional geometrical models for concrete are generated taking the random structure of aggregates at the mesoscopic level into consideration. The generation process is based upon Monte Carlo's simulation method wherein the aggregate particles are generated from a certain aggregate size distribution and then placed into the concrete specimen in such a way that there is no intersection between the particles. For high volume fractions of aggregates, new algorithms for generating realistic concrete models are proposed.

The generated geometrical models are then meshed using the aligned approach in which the finite element boundaries are coincident with materials interfaces and therefore there are no material discontinuities within the elements.

The finite element method (FEM) is used in the direct computation of the effective properties of concrete. The results obtained from the numerical simulations and the subsequent homogenisation are then compared with experimental data. Furthermore numerical simulations of the damage and fracture process of concrete are performed using an isotropic damage model to model the progressive degradation of concrete. Finally, a concrete block is investigated where numerical and experimental results are discussed.

© 2005 Elsevier B.V. All rights reserved.

Keywords: Finite element; Homogenisation; Sieve curves; Concrete; Damage

1. Introduction

Concrete is the most widely used construction material in the world due to its good strength and durability relative to its cost. It has a great variety of applications in the field of civil engineering. In building construction, concrete is used for footings, foundations, columns, beams, girders, wall slabs, and all important building elements.

Concrete has a highly heterogeneous microstructure and its composite behaviour is exceedingly complex. Therefore, reliable predictions of the behaviour of the material based exclusively on experimental studies have become limited. For obtaining a deeper understanding, theoretical studies based on micromechanics analysis of the interaction between various components of concrete have been developed for deducing the macroscopic constitutive behaviour of concrete. However, the microstructure and properties of the individual components

of concrete and their effects on the macroscopic material behaviour have not been taken into account. For such details to be included into the computational analysis, concrete needs to be analysed as a multi-scale composite material where the microstructure is realistically simulated. Numerical simulations, coupled with theory and experiment, are considered to be an extremely important tool for successfully examining material properties by means of computational materials science.

In the numerical simulation of concrete at a mesoscopic level it is evident that several parameters such as the shape, size and distribution of coarse aggregates within the mortar matrix significantly influence the mechanical behaviour of concrete. The aim of this work is to generate random mesostructure models of the concrete material at the mesoscopic level based upon given parameters and probability distribution of aggregate particles coordinates and sizes. Then, the generated mesostructure models are to be meshed using an automatic meshing preprocessor for computational testing of the material with the finite element method (FEM) in order to analyse the effects of the mesostructure constituents on the macroscopic response of the concrete material.

* Corresponding author. Tel.: +49 5117622220.

E-mail address: wriggers@ibnm.uni-hannover.de (P. Wriggers).

Several mesoscopic models of concrete structure have been developed for studying the influence of material composition on the overall behaviour. Bazant et al. [1] developed a truss model to simulate realistically the spread of cracking and its localisation. Schorn and Rode [2] studied damage processes of concrete using a framework model. A lattice model presented by Schlangen and van Mier [3] seemed to be a promising tool for the simulation of typical failure mechanism and crack face bridging in concrete. Another approach for simulating the structure of concrete by a finite element mesh has been developed by Wittmann and his co-workers [4–6]. In this approach, mechanical and nonmechanical properties can be more realistically simulated for concrete with different compositions. Wang et al. [7] proposed a procedure for generating random aggregate structures based on the Monte Carlo random sampling principle and then developed a method of mesh generation for studying the nonlinear behaviour of concrete.

In the generation of random concrete structures the shape of aggregate particles has to be taken into account in order to study the effect of aggregate shapes upon the mechanical behaviour of concrete. Aggregate shapes have a significant influence on the stress distribution within the concrete material and, therefore, on the cracks initiation and damage accumulation up to the macroscopic failure. Two-dimensional models were generated by Zaitsev and Wittmann [8] to study crack patterns in concrete using polygonal and circular shapes for aggregates. Wang et al. [7] and Wittman et al. [5] have generated rounded aggregate particles following the morphological law developed by Beddow and Meloy [9]. For angular shapes of aggregate particles, Wang et al. [7] adjusted shapes of randomly generated polygons to have prescribed elongation ratios. However, for three-dimensional models, Bazant et al. [1], Guidoum and Navi [10], Schlangen and van Mier [3] and Schorn and Rode [2] just assumed that aggregate particles have spherical shapes. More recently, Häfner et al. [11], Leite et al. [12] and Zohdi [13] have used ellipsoid functions with varying parameters for obtaining various aggregate shapes. Garboczi [14] described a mathematical procedure using spherical harmonic functions to completely characterise concrete aggregate particles based on three-dimensional images acquired via X-ray tomography.

Aggregate size distribution plays an essential role in concrete mix design and optimisation. A proper selection of aggregate size distribution affects the main properties of concrete such as workability of concrete mix, mechanical strength, permeability and durability. The size distribution of aggregate particles can be either described by means of grading curves or obtained from sieve analysis. Fuller curve is one of the most acceptable grading curves which provide optimal aggregate packing and the best properties of concrete. Consequently, most researchers including Schlangen [15], Schlangen and van Mier [3], van Mier et al. [16] and Wittmann et al. [6] applied the Fuller curve to geometrical modelling of concrete.

In regard to the simulation of aggregate spatial distribution, different techniques have been developed to generate a mesoscopic structure that resembles the real concrete. Bazant et al. [1], Schlangen and van Mier [3], Wittmann et al. [5] and Wang et al. [7] adopted the take-and-place method for generating ran-

dom particle models of low particle volume fractions. De Schutter and Taerwe [17] used another approach for the generation of random concrete structures based on the divide-and-fill method. A stochastic-heuristic algorithm was developed by Leite et al. [12] for generating a more realistic three-dimensional structure of concrete. For achieving very high aggregate volume fraction, van Mier and van Vliet [18] used an alternative algorithm called the random particle drop method for arrangement of aggregate particles. A different approach called the distinct element method was developed and extensively applied by Cundall and Strack [19] for simulating the behaviour of granular solids such as sand.

Numerical analysis of heterogeneous materials using the FEM requires the discretisation of the created mesoscopic models. Different meshing techniques have been applied for the discretisation of complex microstructures. Aligned meshing approaches have the advantage of explicitly representing the boundaries between particles and matrix. However, the mesh generation of random heterogeneous materials is rather a tedious process in three dimensions. The aligned approach has been used by several authors, e.g. [17,20–22,7,6] for generating finite element meshes in two-dimensional cases. In recent years, it has been recognised that the interfacial transition zone (ITZ) between aggregates and mortar has a great influence on the initiation of microcracks in concrete. Wang et al. [7] developed a mesh generation method based on the advancing front approach in which the ITZ domains are modelled using Goodman type elements. However, Eckardt et al. [20] disregarded the ITZ and assumed that the bond between aggregates and mortar is rigid.

Schlangen and van Mier [3] and Schorn and Rode [2] used a projection method of a regular mesh onto the random aggregate structure. In the models of van Mier and van Vliet [18], van Mier et al. [16], Schlangen [15] and Schlangen and van Mier [3] the aggregates, matrix and ITZ properties are assigned to a lattice of beam elements. A similar technique has been applied by Leite et al. [12] in which the models are idealised as planar trusses and frames for two-dimensional analyses while for three-dimensional analyses the models are idealised as space structures. An alternative approach has been introduced by Zohdi and Wriggers [23] who used cubic meshes for testing mechanical responses of random heterogeneous materials. In this an unaligned approach the number of integration points is increased in order to better capture the geometry in elements with material discontinuities. Also, a quite good approximation of the geometry of heterogeneous materials has been recently obtained by Löhnert [24] using the hanging node concept in which the mesh is refined close to the geometrical boundaries of the inclusions and the cohesive zone.

2. Concrete mesostructure

In computational material science, concrete is characterised as a multi-phase material with several different representative scales. At macroscopic scale, concrete could be regarded as a homogeneous material while at mesoscopic scale it is treated as consisting of coarse aggregates and mortar matrix. Further

subdivisions of the mortar matrix produce fine aggregates and hardened cement paste with pores embedded inside. More details on length scales of concrete can be found in the literature (see for instance [25,21]). Mesoscopic models have proven to be the most practicable and useful approach for studying the influence of the concrete composition on the macroscopic properties [7] and also to gain insight into the origin and nature of the nonlinear behaviour of concrete. In the following, the most recent computer-based models for describing mesostructure of concrete are presented.

A “numerical concrete” model was first developed by Wittmann et al. [5] in order to represent concrete mesostructure numerically within a computer. A concrete mesostructure consisting of aggregates and cement paste matrix was first generated and then mapped onto a finite element grid. Each aggregate particle could be mapped onto one or more finite elements, so that the “numerical model” represented the concrete at the subparticle level.

Concrete mesostructure models could be generally classified as a continuum-based model at particle level and a digital-based model at subparticle level. Continuum-based models can provide valuable quantitative information, such as the effects of particle size on hydration kinetics, but it is very difficult to analyse such a mesostructure to directly compute system transport and elastic properties (see [26,27] for review).

Digital-based models [28] represent each cement particle as a collection of elements (pixels) and, therefore, mapping the mesostructure onto a finite difference or finite element grid becomes trivial due to the simple one-to-one mapping between pixels and finite elements. However, the major limitation of such models is mainly the resolution problem, because each pixel is typically $1\ \mu\text{m}^3$ in volume and features smaller than that cannot be resolved. Further investigation can be found in [29].

2.1. Mesostructure generation

The evaluation of the composite behaviour of concrete at mesoscopic level requires the generation of a random aggregate structure (Fig. 1) in which the shape, size and distribution of the coarse aggregate closely resemble real concrete in the statistical sense. This structure to be generated consists of randomly distributed aggregate particles and mortar matrix filling the space between the particles. The layout of the matrix material is dependent entirely on the spatial distribution of the aggregate particles. Therefore, one does not need to consider it separately.

The generation of the random geometrical configurations of the aggregate particles must satisfy the basic statistical characteristics of the real material. Also, the spatial distribution of the aggregate particles must be as macroscopically homogeneous in space and macroscopically isotropic as possible [1]. In order to produce the geometrical configuration which meets these requirements, the random sampling principle of Monte Carlo’s simulation method is used. This random principle is applied by taking samples of aggregate particles from a source

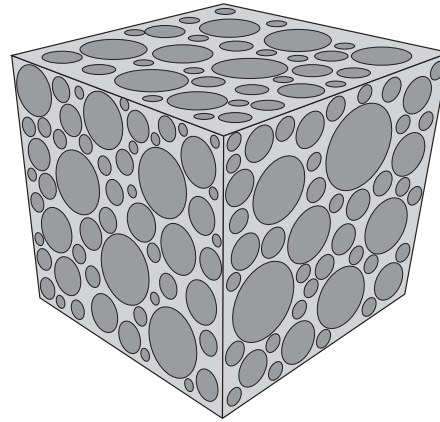


Fig. 1. Concrete mesostructure.

whose size distribution follows a certain given grading curve and placing the aggregate particles one by one into the concrete in such a way that there is no overlapping with particles already placed. This method has been used by most researchers including Bazant et al. [1], Schlangen and van Mier [3], Wang et al. [7] and Wittmann et al. [5] with varying degrees of sophistication and is commonly called the take-and-place method while De Schutter and Taerwe [17] used the divide-and-fill method. A different approach, the distinct element method, has been used by Cundall and Strack [19] to simulate actually the production of the material.

Here, taking into account the power of computer facilities available today, a new algorithm for generating a realistic aggregate structure is proposed. In this algorithm whenever the placing process of a particle reveals an overlapping, the particle being placed is *translated* the least distance allowed between the particles in order to get away from the overlapping particle. With keeping this distance constant, the particle is then randomly *rotated* in order to search for a free position around the overlapping particle until all the placing requirements are completely satisfied. The algorithm shows that fast and good results can be obtained in generating aggregate contents comparable to the ones in real concrete and equivalent spatial distributions.

2.2. Generation of aggregate particles

Aggregates generally occupy 60–80% of the volume of concrete and greatly influence its properties, mix proportions and economy. Sand, gravel and crushed stone are the primary aggregates used. Aggregates are divided into two distinct categories, fine and coarse aggregates. Fine aggregates generally consist of natural sand or crushed stone with most particles passing through a 4.75-mm sieve. Coarse aggregates are any particles greater than 4.75 mm in diameter. For most concrete, the coarse aggregate represents around 40–50% of the concrete volume. Gravels constitute the majority of coarse aggregate used in concrete with crushed stone making up most of the remainder.

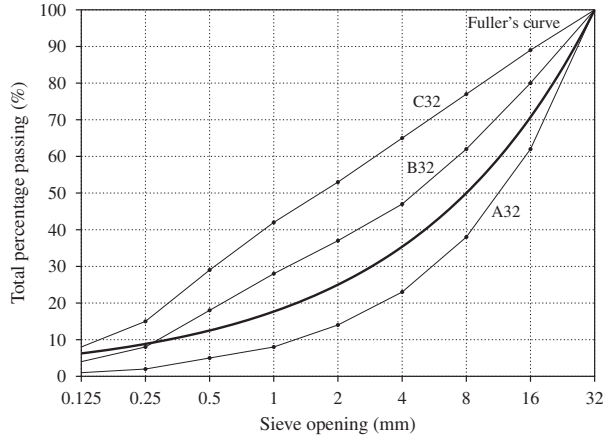


Fig. 2. Fuller and limiting grading curves.

The shape of aggregate particles depends on the aggregate type. In general, gravel aggregates have a rounded shape while crushed stone aggregates have an angular shape [7]. Several attempts to characterise the geometry of aggregates have been published. Wang et al. [7] and Wittmann et al. [5] have used the morphological law developed by Beddow and Meloy [9] for generating gravel aggregates. Spherical shape for aggregate particles was assumed by others [1–3]. Further details on generating the geometry of aggregates can be found in the literature, e.g. Häfner et al. [11], Roelfstra [30], Wang et al. [7], Wittmann et al. [5] and Zohdi [13].

Here, for the sake of simplicity, it is assumed that aggregate particles have spherical shapes.

2.2.1. Aggregate size distribution

Grading refers to the determination of the particle size distribution for aggregate, usually expressed in terms of cumulative percentage passing through a series of sizes of sieve openings. This can be reflected by formulas, tables or graphics. One of the most known and acceptable aggregate distribution is given by Fuller, which also lies within the proposed limiting grading curves A32 and B32 of DIN 1045 (Fig. 2). In practice, concrete is most designed after Fuller curve which represents a grading of aggregate particles resulting in optimum density and strength of the concrete mixture. Fuller curve can be described by a simple equation

$$P(d) = 100 \left(\frac{d}{d_{\max}} \right)^n, \quad (1)$$

where $P(d)$ is the cumulative percentage passing a sieve with aperture diameter d , d_{\max} is the maximum size of aggregate particles and n is the exponent of the equation ($n = 0.45$ – 0.70).

In a concrete mix, the amount of coarse aggregate is normally given in terms of weight per unit volume of concrete. Therefore, one can obtain the volumetric ratio of coarse aggregate content by dividing the weight of coarse aggregate per volume of concrete by the density of the aggregate [7].

This can be defined as

$$v_p = \frac{w_p}{\rho_p V}, \quad (2)$$

where v_p is the volume fraction of aggregate, w_p is the total weight of aggregate particles, ρ_p is the specific weight and V is the total volume of the specimen.

If the size distribution of the aggregate particles is given by one of the common grading curves, then the amount of aggregate within the grading segment $[d_s, d_{s+1}]$ can be calculated as

$$V_p[d_s, d_{s+1}] = \frac{P(d_s) - P(d_{s+1})}{P(d_{\max}) - P(d_{\min})} \times v_p \times V, \quad (3)$$

where $V_p[d_s, d_{s+1}]$ is the volume of aggregate within the grading segment $[d_s, d_{s+1}]$, d is the aperture size of the sieve, d_{\min} and d_{\max} are the minimum and maximum sizes of coarse aggregate particles, respectively.

2.2.2. Taking process

After dividing the grading curve into segments, the taking process starts with the grading segment containing the largest size particles. Then the aggregate particles within the grading segment are generated in the following procedure:

- Step 1. Calculate the volume of aggregate to be generated in the grading segment.
- Step 2. Generate a random number defining the size of an aggregate particle. Assuming that the size d has a uniform distribution between d_s and d_{s+1} , it may be calculated using the following expression:

$$d = d_{s+1} + \eta(d_s - d_{s+1}), \quad (4)$$
 where η is a random number uniformly distributed between 0 and 1.
- Step 3. Calculate the volume of the generated aggregate particle and subtract it from the volume of aggregate within the grading segment.
- Step 4. Repeat steps 2 and 3 until the volume of aggregate left to be generated is less than $\frac{4}{3}\pi(d_{s+1}/2)^3$, i.e. not enough for generating another particle. The remaining volume of aggregate to be generated is then transferred to the next grading segment.
- Step 5. Repeat all the above steps for the next smaller size grading segment and then again for successively smaller size grading segment, until the last particle of the smallest size has been generated.

Fig. 3 shows the programming algorithm for generating the aggregate particles depending on a given particle size distribution.

2.2.3. Placing process

The concrete volume whose random configuration is to be generated may have a cubical, cylindrical or even arbitrary shape depending on the type of concrete specimen to be studied. In this research, the generation of the random aggregate configuration will be restricted to specimens of a cubical form.

```

divide grading curve into  $m$  segments
initialise variables
 $V_r$ : remaining volume
 $n_g$ : number of generated particles
for  $s = 1, \dots, m$  do
 $V_p = \frac{P(d_s) - P(d_{s+1})}{P(d_{max}) - P(d_{min})} \times v_p \times V$ 
 $V_s = V_p + V_r$ 
set  $V_r = V_s$ 
while  $V_r \geq \frac{3}{4}\pi \left(\frac{d_{s+1}}{2}\right)^3$  do
    generate random number  $\eta$ 
 $d = d_{s+1} + \eta(d_s - d_{s+1})$ 
 $V_p = \frac{3}{4}\pi \left(\frac{d}{2}\right)^3$ 
 $V_r = V_r - V_p$ 
 $n_g = n_g + 1$ 
end while
end for
stop
    
```

Fig. 3. Programme flowchart of taking process.

A cartesian coordinate system x_i is used in the concrete specimen. When a particle is placed into the concrete volume, its position is defined by \mathbf{x} of a reference point O which is taken to be the centre of the particle. Assuming a uniform probability distribution for the location of O throughout the concrete volume, the coordinates of O may be obtained as

$$\mathbf{x} = \mathbf{x}_{min} + \boldsymbol{\eta}(\mathbf{x}_{max} - \mathbf{x}_{min}), \quad (5)$$

where \mathbf{x} is the position vector of O , \mathbf{x}_{min} and \mathbf{x}_{max} are the minimum and maximum coordinates of the concrete volume, and $\boldsymbol{\eta}$ are three independent random numbers uniformly distributed between 0 and 1.

In order to place an aggregate particle at a free position within the concrete volume, two obvious conditions need to be satisfied. Firstly, the whole particle must be completely within the boundary of the concrete volume. Secondly, there must not be any overlapping with previously placed particles.

In addition to these two conditions, there is a third condition that each particle must be coated all around with a mortar film having a certain minimum thickness. This implies that there is a minimum distance between the edge of a particle and the boundary of the concrete specimen and a minimum gap width between two adjacent particles. A value of $0.1(d_a + d_b)/2$, where d_a and d_b are the sizes of the two particles, was proposed by Schlangen and van Mier [3] to be used for the minimum gap width between adjacent particles. However, Wittmann et al. [5] found that the thickness of the average mortar film between aggregate particles varies with the aggregate content, being smaller when the aggregate content is higher. Also, Wang et al. [7] have investigated the thickness of the mortar film

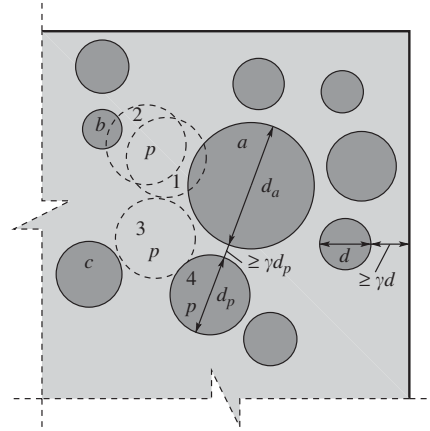


Fig. 4. Placing process.

coating an aggregate particle through visual inspection of cross sections of hardened concrete. It revealed that the thickness of the mortar film is more or less proportional to the particle size. Hence, it is proposed that the minimum thickness of the mortar film between a particle of size d and the concrete boundary be taken as γ times d , and the minimum thickness of the mortar film between two particles be taken as γ times the size of the particle being placed (Fig. 4), where γ is a distribution factor whose value is dependent on the aggregate volume fraction.

This distribution factor γ plays a significant role in the spatial configuration of the aggregate particles. As a larger value of γ is used, a more uniform spatial distribution of the particles will be obtained but it could also lead to difficulties in finding enough space to place the particles. On the other hand, when a smaller value of γ is used, an easier packing of the particles into the concrete can be obtained but the generated configuration would be macroscopically less homogeneous. At the beginning of the placing process, an initial value of γ is chosen depending on the volume fraction of aggregate. Whenever there are difficulties with placing the particles, the value of γ is reduced and the whole placing process is repeated. If the same difficulties arise again, the value of γ is further reduced and so on until all the particles can be placed into the concrete.

The third condition can be checked concurrently with the checking of the first two conditions. This can be done when checking the first condition by enlarging the size of the particle to $(1 + \gamma)$ times its size and when checking the second condition by enlarging the size of the particle being placed by the same factor.

The whole adopted procedure of the placing process can be summarised in the following steps:

- Step 1. Random numbers defining the position of the aggregate particle are generated.
- Step 2. Checking whether all the placing conditions are completely satisfied.

Step 3. If checking of these conditions reveals that any of them is violated, the particle is not placed into the concrete. In case the violation is due to the first condition, then another set of random numbers is generated for \mathbf{x} and an attempt of placing the particle at a new location is made, whereas in the other case, in which the second condition is not satisfied, then the translation–rotation algorithm is followed (see Section 2.1). Using spherical coordinates (ρ, θ, ϕ) located at the centre of the overlapping particle, the new coordinates can be calculated as

$$\begin{aligned}\bar{x}_1 &= \rho \cos \theta \sin \phi + x_1, \\ \bar{x}_2 &= \rho \sin \theta \cos \phi + x_2, \\ \bar{x}_3 &= \rho \cos \phi + x_3,\end{aligned}\quad (6)$$

where the spherical coordinates of the particle may be obtained as

$$\begin{aligned}\rho &= s + \gamma r, \\ \theta &= \zeta 2\pi, \\ \phi &= \xi \pi,\end{aligned}\quad (7)$$

where s is the distance between the particles, r is the radius of the particle, ζ and ξ are different random numbers.

Step 4. If the translated particle cannot satisfy the placing conditions after a prescribed number of trials, new random numbers are generated for \mathbf{x} to make another effort for placing the particle.

Step 5. If the particle cannot be placed into the concrete specimen after an appropriate number of trials for \mathbf{x} , the whole placing process is stopped and all particles previously placed into the concrete are cleared. The value of γ is then reduced and the whole placing process is restarted.

Step 6. The steps described above are repeated until all the particles are successfully placed into the concrete specimen.

2.2.4. Re-generation algorithm

There are some cases where the minimum value of the distribution factor is reached but not all the aggregate particles have been placed into the concrete volume. This usually occurs when bad grading curves are used in the taking process. In order to cope with such a difficulty, a re-generation of the remaining particles is made. In the re-generation process, new aggregate particles with smaller sizes are generated from the remaining particles. These new aggregate particles must be generated within the grading segment which the remaining particles belong to, so the same volume of aggregate in that segment is obtained. The main reason of re-generating particles having smaller sizes is to ensure that they are successfully packed into the tight spaces left between the placed particles.

Table 1
Results of aggregate sieve analysis

Aggregate type	Sieve size (mm)	Total percentage retained (%)	Total percentage passing (%)
I	12.70	0	100
	9.50	23	77
	4.75	74	26
	2.36	100	0
II	19.00	0	100
	12.70	3	97
	9.50	39	61
	4.75	90	10
	2.36	98.6	1.4

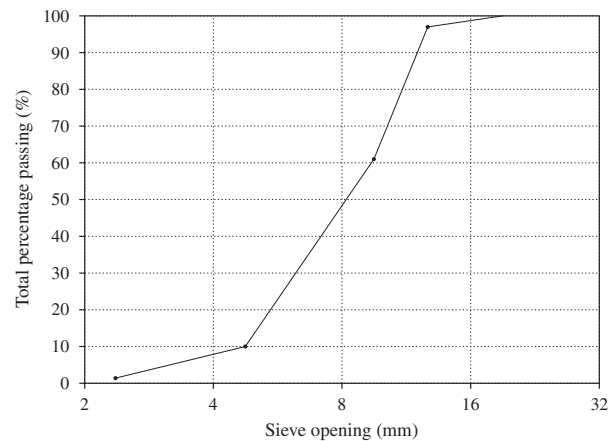


Fig. 5. Particle size distribution curve.

2.3. Mesostructure models

Here are some geometrical models of random aggregate distributions generated using sieve analysis data as well as Fuller curve for aggregate gradation. All generation processes were run on a standard PC (2.0 GHz, Pentium IV) available in most academic places. These models will be used later to determine the concrete effective properties and also to investigate the behaviour of concrete at the mesoscopic scale.

2.3.1. Sieve analysis models

Several types of aggregate were selected for use in concrete mix. The results of aggregate sieve analysis found in Hirsch [31] are given in Table 1.

Fig. 6 shows some generated mesostructure models of concrete for the aggregate grading curve of the aggregate type II (Fig. 5). Fig. 6(a) shows a mesostructure of aggregate particles with 20% volume fraction and 216 aggregate particles. The value of the distribution factor γ is 0.46 and the computing time for generating the model is approximately 5 s. Fig. 6(b) represents a 30% volume fraction mesostructure with 338 aggregate particles. The evaluated γ is 0.18 whereas the computing time for this model is about 920 s. In Figs. 6(c) and (d), higher

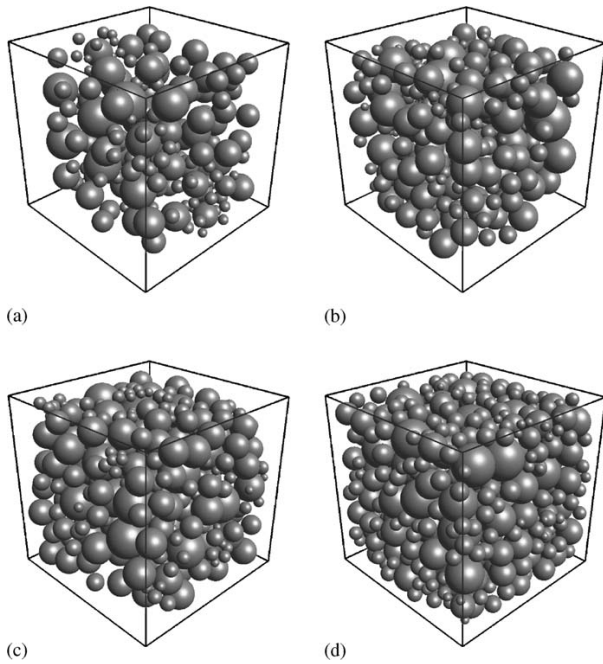


Fig. 6. Models based on sieve analysis. (a) $v_p = 20\%$, $\gamma = 0.46$, (b) $v_p = 30\%$, $\gamma = 0.18$, (c) $v_p = 40\%$, $\gamma = 0.02$, (d) $v_p = 50\%$, $\gamma = 0.02$.

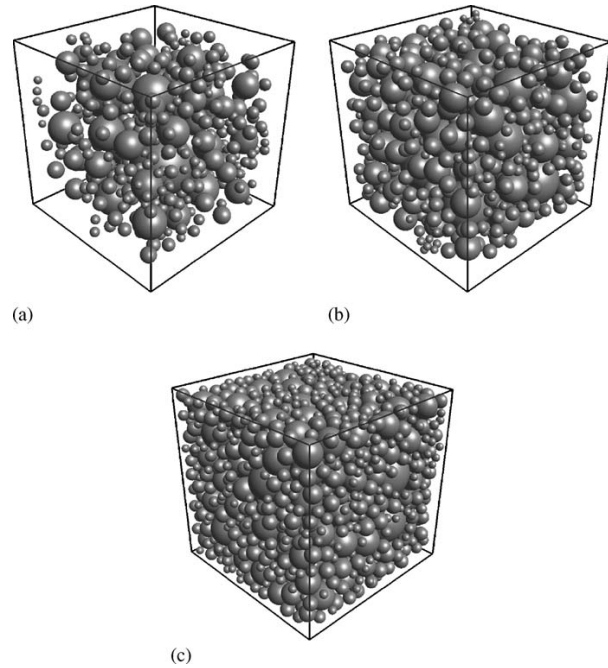


Fig. 7. Models based on Fuller curve. (a) $v_p = 20\%$, $\gamma = 0.68$, (b) $v_p = 40\%$, $\gamma = 0.20$, (c) $v_p = 60\%$, $\gamma = 0.02$.

values of v_p are used in order to generate denser mesostructures of aggregate particles. In case of 40% volume fraction, the consuming time for generating and placing 466 aggregate particles is 1135 s with $\gamma = 0.02$. The re-generation process of aggregate particles is required for generating the 50% volume fraction mesostructure where the smallest value of the distribution factor ($\gamma = 0.02$) is reached and, therefore, the required computing time increases to 1345 s.

2.3.2. Fuller curve models

Aggregate arrangements of the models generated here are based on Fuller curve using Eq. (1) with $n=0.50$. The aggregate sizes used in these models are 2.36–19.0 mm.

In Fig. 7(a) approximately 2.55 s are required for generating the mesostructure of 405 aggregate particles with $\gamma = 0.68$. In the model of 40% volume fraction shown in Fig. 7(b) the computing time of the generation process increases to 7.14 s. The final value of γ required to randomly place 794 aggregate particles within the specimen of cubical shape is 0.20. Fig. 7(c) shows a generated mesoscopic model with aggregate volume fraction of 60%. The model consists of 1794 aggregate particles which require approximately 10 142 s to be successfully placed within the cube.

It is to be noted that the generation process of the models using Fuller curve requires less time compared with the ones based on the sieve analysis. This is due to the fact that the aggregate gradation based on Fuller curve gives an optimal packing of aggregates and, as a consequence, results in a greater number of aggregate particles with small sizes. Therefore, it is

rather an easy task for the generation process to place small aggregate particles within spaces between aggregate particles of bigger sizes.

3. Micromechanics concepts

Concrete is a quite complicated composite material with a variety of heterogeneities. Determination of the macroscopic response of such heterogeneous materials is of a great interest in engineering applications and extensive research has been made in the last 150 years [32]. The main interest is to compute a relation between the microscopic deformation and the macroscopic mechanical behaviour. A method for obtaining such a relation is referred to as *homogenisation* or *theory of effective properties*, by which the heterogeneous material is replaced by an equivalent homogeneous continuum. The method is performed on a statistically representative sample of material, referred to as a representative volume element (RVE), see e.g. Aboudi [33], Hill [34] and Zohdi and Wriggers [32].

Early approximations for the effective properties of heterogeneous materials were first developed by Voigt [35], Reuss [36] and Hill [37]. In 1957, Eshelby [38] obtained a relatively compact solution which has been a basis for many approximation methods. Based on variational principles, Hashin and Shtrikman [39] have developed a model which improved solutions of the effective properties. More classical models have been proposed to estimate the effective properties, including the self-consistent method, the Mori and Tanaka [40] method and so on (see [41] for review).

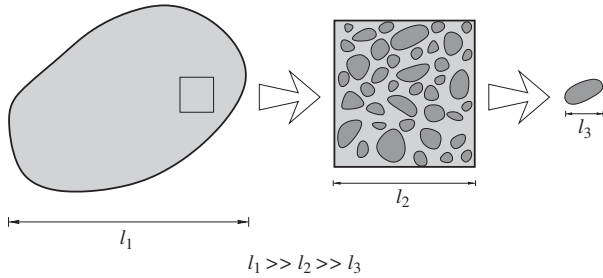


Fig. 8. Size requirements of RVE.

Unfortunately, most of these analytical models can only give estimates or bounds for the effective properties, and the simplifying assumptions used sometimes result in considerable differences in the predictions. Considering that full experimental characterisation of effective material properties is not always feasible and also the recent increase in computer power, some numerical simulations have been conducted using different methods. One of the most efficient numerical methods is the FEM, whereby the effective responses can be obtained by volumetrically averaging numerical solutions of RVEs [32,42].

In the classical approximations of the effective response of heterogeneous materials the size of the RVE is usually considered to be infinitely large in comparison to the length scales of the microstructure. However, only samples with finite sizes can be practically tested for computing the effective properties of heterogeneous materials with random microstructures. Such difficulties and also due to the recent increase in computer power have led to direct numerical simulations wherein the need for most approximation methods is eliminated. In these direct methods, such as the FEM, the effective responses can be obtained by volumetrically averaging the internal fields over an RVE of the heterogeneous material. In the following, the fundamental theorems of the computational process will be illustrated.

3.1. Hill's energy condition

For a body with perfectly bonded constituents and no body forces, the Hill's condition states that

$$\langle \epsilon \rangle_{\Omega} : \langle \sigma \rangle_{\Omega} = \langle \epsilon : \sigma \rangle_{\Omega} \quad (8)$$

which dictates that for a sample to be statistically representative, it should be large compared to the scales of microstructure, but is still small compared to the entire body (Fig. 8). For the special cases of homogeneous strain and stress boundary conditions, the sample must be large enough for boundary field fluctuations to be relatively small. Hill's condition implies that the volume averaged strain energy density of a heterogeneous material can be obtained from the average stress and strain, provided that the micro-macroscales are sufficiently different.

More details and complete derivations of homogenisation and average theorems can be found in the literature, e.g. Aboudi

[33], Christensen [43], Hashin [44], Nemat-Nasser and Hori [45] and [42].

3.2. Effective material properties

In order to computationally simulate the effective response of concrete, three-dimensional samples of different aggregate distributions and volume fractions are generated. Then, under a given set of specified boundary loadings applied on these samples, variational boundary value problems are obtained and solved using the FEM.

Thus, for determining the effective elastic properties of concrete, the constitutive relation between averages is computed. In a matrix form

$$\begin{Bmatrix} \langle \sigma_{11} \rangle_{\Omega} \\ \langle \sigma_{22} \rangle_{\Omega} \\ \langle \sigma_{33} \rangle_{\Omega} \\ \langle \sigma_{12} \rangle_{\Omega} \\ \langle \sigma_{23} \rangle_{\Omega} \\ \langle \sigma_{31} \rangle_{\Omega} \end{Bmatrix} = \begin{bmatrix} C_{11}^* & C_{12}^* & C_{13}^* & C_{14}^* & C_{15}^* & C_{16}^* \\ C_{21}^* & C_{22}^* & C_{23}^* & C_{24}^* & C_{25}^* & C_{26}^* \\ C_{31}^* & C_{32}^* & C_{33}^* & C_{34}^* & C_{35}^* & C_{36}^* \\ C_{41}^* & C_{42}^* & C_{43}^* & C_{44}^* & C_{45}^* & C_{46}^* \\ C_{51}^* & C_{52}^* & C_{53}^* & C_{54}^* & C_{55}^* & C_{56}^* \\ C_{61}^* & C_{62}^* & C_{63}^* & C_{64}^* & C_{65}^* & C_{66}^* \end{bmatrix} \begin{Bmatrix} \langle \epsilon_{11} \rangle_{\Omega} \\ \langle \epsilon_{22} \rangle_{\Omega} \\ \langle \epsilon_{33} \rangle_{\Omega} \\ 2\langle \epsilon_{12} \rangle_{\Omega} \\ 2\langle \epsilon_{23} \rangle_{\Omega} \\ 2\langle \epsilon_{31} \rangle_{\Omega} \end{Bmatrix} \cdot \quad (9)$$

To solve for all 36 components in the effective elastic tensor C^* , six linearly independent boundary conditions have to be specified. However, due to the idealisation of the homogenised behaviour of concrete as being statistically isotropic, only one loading state is sufficient for describing the overall linear elastic behaviour. Thus, the effective bulk and shear moduli are given by

$$3\kappa^* = \frac{\langle \text{tr } \sigma / 3 \rangle_{\Omega}}{\langle \text{tr } \epsilon / 3 \rangle_{\Omega}} \quad \text{and} \quad 2\mu^* = \sqrt{\frac{\langle \hat{\sigma} \rangle_{\Omega} : \langle \hat{\sigma} \rangle_{\Omega}}{\langle \hat{\epsilon} \rangle_{\Omega} : \langle \hat{\epsilon} \rangle_{\Omega}}}, \quad (10)$$

where κ^* is the effective bulk modulus, μ^* is the effective shear modulus and $\hat{\sigma} = \sigma - (\text{tr } \sigma / 3)\mathbf{I}$ and $\hat{\epsilon} = \epsilon - (\text{tr } \epsilon / 3)\mathbf{I}$ are the deviatoric parts of σ and ϵ , respectively.

3.3. Testing process

In this section the effective properties of concrete are determined for the RVEs generated in Section 2. For the numerical models to be consistent, the results obtained from numerical simulations are compared with experimental data found in the literature.

3.3.1. Results of sieve analysis

In the determination of the effective properties the results for each aggregate type are averaged over 10 tests with the same

Table 2
Material data of constituents

Material property	Mortar material	Aggregate material	
		I	II
E (GPa)	19.0	72.0	62.0
ν	0.20	0.20	0.20

Table 3
Elastic modulus of concrete

Aggregate type	Volume fraction (%)	Modulus of elasticity E (GPa)	
		Numerical	Experimental
I	20	24.233	26.130
	30	27.462	30.750
	40	31.331	35.300
	50	35.774	37.440
II	20	23.634	22.960
	30	26.493	27.440
	40	29.857	29.720
	50	33.455	32.540

aggregate volume fraction but different aggregate distributions. Uniform displacement boundary conditions of the form

$$\mathbf{u}|_T = \epsilon^0 \cdot \mathbf{x} \quad \text{with} \quad \epsilon^0 = \begin{bmatrix} 0.001 & 0.001 & 0.001 \\ 0.001 & 0.001 & 0.001 \\ 0.001 & 0.001 & 0.001 \end{bmatrix} \quad (11)$$

are applied at the boundaries of the RVEs. Once the average stresses and strains are obtained from the direct computational method using the FEM, the effective properties are computed using Eq. (10).

Table 2 gives the material data of the mortar and aggregate materials. Experimental data of elastic modulus of concrete found in Hirsch [31] and the effective properties of concrete computed from the numerical simulations are given in Table 3.

In the experimental investigation of Hirsch [31] several types of aggregates were selected for use in concrete mixes. Various proportions of these aggregates were mixed with a selected cement paste in order to observe the effects of their elastic moduli and of batch proportions on the elastic modulus of concrete. No attempt was made in this investigation to evaluate the effects of size, shape, texture and gradation of the aggregates on the elastic moduli of concrete. The secant moduli of concrete specimens were determined from stress–strain curves as given by the slope of a straight line drawn from the point of zero stress to a stress of 6.9 GPa.

In Fig. 9 it can be seen that the numerical results for the aggregate type I underestimate the elastic modulus of concrete with aggregate volume fractions of 20%, 30% and 40%. The relative error for these volume fractions is 7.26%, 10.69% and 11.24%, respectively. It is obvious that the relative error increases as a function of the aggregate volume fraction. However, a smaller relative error of value 4.45% is obtained in the case of the 50% volume fraction. In addition, the solutions of the finite element analysis are compared with the classical

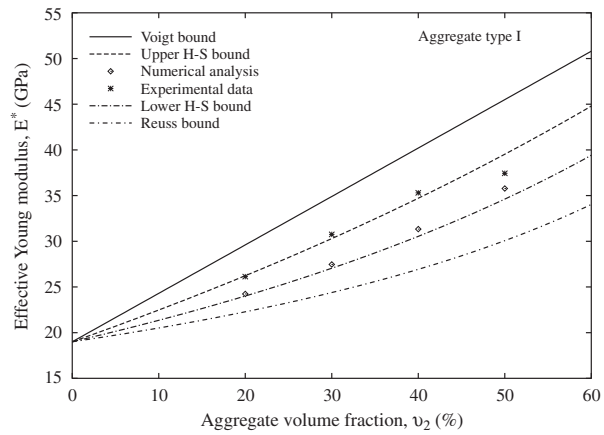


Fig. 9. Young’s modulus using aggregate type I.

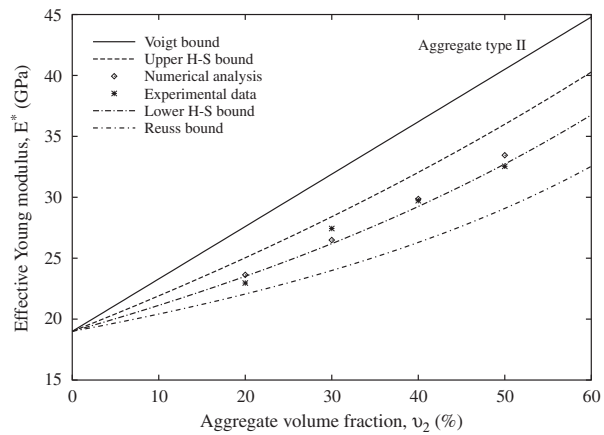


Fig. 10. Young’s modulus using aggregate type II.

bounds of Hashin and Shtrikman [39], Hashin and Shtrikman [46], Reuss [36] and Voigt [35] which give a theoretical range of the effective elastic modulus of concrete with respect to a certain volume fraction of the constituents.

A better estimations of the elastic modulus of concrete for the aggregate type II are shown in Fig. 10. At a volume fraction of 40% the numerical model leads to identical results of the experiments. However, the finite element responses for 20% and 40% volume fractions tend to be stiffer than the experimental ones with a relative error of value 2.9%. It is clearly seen that these predictions of the elastic modulus of concrete are much closer than the ones of the aggregate type I. This is probably due to the different shapes of aggregates which have angular shapes in type I while the aggregate type II have rounded ones just as it has been assumed in the numerical model.

3.3.2. Results of Fuller curve

The same procedure is followed here in computing the effective modulus of elasticity. Material properties and experi-

Table 4
Material properties of concrete

Material type	Material properties		Volume fraction (%)	Modulus of elasticity E (GPa)	
	E (GPa)	ν		Numerical	Experimental
Mortar	11.6	0.20	20	15.760	15.800
			40	22.150	23.200
Aggregate	74.5	0.20	60	32.058	30.700

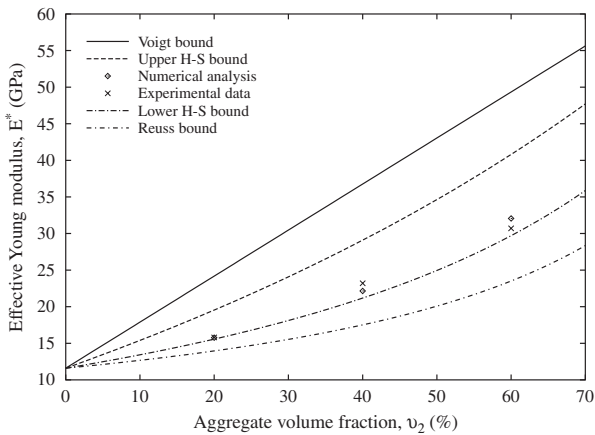


Fig. 11. Young's modulus based on Fuller curve.

mental data found in Stock et al. [47] are given in Table 4. In the experimental tests the aggregate sizes of 0.15–19 mm were used while in the numerical model the smallest aggregate size is 2.36 mm. Different aggregate volume fractions of values 20–80% were used in the tests to study their effects on the strength and elastic modulus of concrete. A good aggregate distribution was achieved by applying a vibration technique in various positions. Elastic modulus of concrete was measured on cylindrical specimens of 100 mm in diameter and 300 mm in length. The modulus of elasticity was determined by the secant to 33% of the ultimate stress in compression.

Finite element analyses of RVEs based on Fuller curve give generally good results in comparison with the experimental data of Stock et al. [47]. Fig. 11 shows that the effective modulus of elasticity obtained from the numerical model is identical to the experimental one for aggregate volume fraction of 20%. For higher volume fractions, the maximum relative error of the data is approximately 4.5%. Numerical models with 60% volume fraction have stiffer responses than the ones obtained from experiments. This is possibly due to the increasing volume of ITZ as a function of the aggregate volume fraction whereas it has been excluded in the numerical modelling.

In summary, the results of the finite element analysis are in a good agreement to the experimental data of Hirsch [31] for aggregate type II and also to the results obtained by Stock et al. [47]. In addition, all the computed results of RVEs are completely within the classical bounds of Hashin and Shtrikman

[39], Hashin and Shtrikman [46], Reuss [36] and Voigt [35] in spite of the fact that these bounds are usually applicable to samples of infinitely large sizes. An improvement in predicting the elastic modulus of concrete would probably be reached with an inclusion of the ITZ in the modelling for high volume fractions of aggregate. Also, the numerical computations show a possible influence of the aggregate shape on the overall properties of concrete. Thus, a three-dimensional simulation of the aggregate various shapes is unavoidable in future work to see whether shape variations have any significant effect on the effective elastic parameters of concrete.

4. Concrete damage

Numerical simulation of the damage and fracture process of concrete has evolved considerably over the past years. Research on the fracture of concrete subjected to a variety of external loadings is very necessary for developing more efficient concrete for engineering use. It has been generally accepted that the deformation of concrete is associated with very complicated progressive failures, as characterised by initiation, propagation and coalescence of microcracks due to its heterogeneity. In the next section a brief review of models used to simulate the fracture process in concrete is given. For more details on the modelling of fracture process in concrete, see e.g. Carpinteri and Aliabadi [48], Lemaitre [49], Lemaitre and Sermage [50], Fanning and Kelly [51] and Rots [52].

In the past classical mathematical models based on elasticity, plasticity and viscoelasticity formulations were used for describing the nonlinearity of concrete. In the 1970s models based on nonlinear fracture mechanics and continuum damage mechanics were developed for simulating the crack propagation and the degradation of the material stiffness in concrete. However, these classical models generally neglect the heterogeneity of concrete and consider it as a homogenised material. These kinds of homogenisation are incapable of characterising the entire fracture process from initialisation, propagation and coalescence of microcracks to the formation of macrocracks in concrete. Moreover, these models cannot reflect the randomness of concrete mesostructure properties and consequently are insufficient for developing a comprehensive understanding of the fracture process of concrete. Therefore, different numerical models for the simulation of the fracture process in concrete at the mesoscale have been proposed in recent years. For instance, Bazant et al. [1] presented a random particle model for fracture of brittle aggregate composite materials. In this model the matrix material is described by a softening stress–strain relation corresponding to a prescribed microscopic interparticle fracture energy. In the lattice model of Schlangen and Garboczi [53] and Schlangen and van Mier [3] tensile strengths are given to the lattice elements in order to simulate the fracture mechanism in heterogeneous materials such as concrete. The lattice model was extended by Lilliu and van Mier [54] for three-dimensional analyses. Eckardt et al. [20] described the fracture behaviour of the aggregates and the matrix using the smeared crack concept and observed reasonable crack patterns during the simulations.

4.1. Isotropic damage model

Continuum damage mechanics has been extensively applied to model the progressive degradation of materials caused by microcracking [55]. It has been established that the damage mechanics approach can accurately model the strain-softening response of concrete [56]. These continuum models assume that the local damage in the material can be averaged and represented in the form of damage variables which are related to the tangential stiffness tensor of the material. Krajcinovic [55] as well as Mazars and Pijaudier-Cabot [56] used a scalar damage variable to model isotropic damage based on an experimental stress–strain curve of concrete under uniaxial tension. More information about continuum damage models can be found for instance in Mazars and Pijaudier-Cabot [57] and Peerlings [58]. In this work, the scalar damage model of Mazars [59] is used in modelling the mechanical behaviour of concrete due to its simplicity.

4.1.1. Constitutive law

In this model the stiffness degradation of the material is simply assumed to be isotropic. Consequently, the stress–strain law of elastodamaging materials takes the form

$$\sigma = (1 - D)C\epsilon, \tag{12}$$

where the damage scalar D ranges from 0 for the undamaged material to 1 for completely damaged material. The elastic energy per unit mass of material is

$$\rho\psi = \frac{1}{2}(1 - D)\epsilon C \epsilon \tag{13}$$

which is assumed to be the state potential. The damage energy release rate is

$$Y = -\rho \frac{\partial \psi}{\partial D} = \frac{1}{2}\epsilon C \epsilon \tag{14}$$

with the rate of dissipated energy

$$\dot{\phi} = -\rho \frac{\partial \psi}{\partial D} \dot{D}. \tag{15}$$

Since the dissipation of energy ought to be positive or zero, the damage rate is constrained to the same inequality because the damage energy release rate is always positive.

4.1.2. Evolution of damage

The evolution of damage is based on the amount of extension that the material is experiencing during the mechanical loading. It is assumed that the damage to be governed by the equivalent strain defined as

$$\tilde{\epsilon}(\epsilon) = \sqrt{\sum_{i=1}^3 \langle \epsilon_i \rangle_+^2}, \tag{16}$$

where $\langle \cdot \rangle_+$ is the Macauley bracket and ϵ_i are the principal strains. The loading function of damage is

$$f(\tilde{\epsilon}, \kappa) = \tilde{\epsilon} - \kappa, \tag{17}$$

where κ is threshold of damage growth. Initially, its value is κ_0 , which can be related to the peak stress f_t of the material in uniaxial tension

$$\kappa_0 = \frac{f_t}{E}. \tag{18}$$

In the course of loading κ assumes the maximum value of the equivalent strain ever reached during the loading history.

$$\text{If } f(\tilde{\epsilon}, \kappa) = 0 \text{ and } \dot{f}(\tilde{\epsilon}, \kappa) = 0, \text{ then} \tag{19}$$

$$\begin{cases} D = g(\kappa) \\ \kappa = \tilde{\epsilon} \end{cases} \text{ with } \dot{D} \geq 0 \text{ else } \begin{cases} \dot{D} = 0, \\ \dot{\kappa} = 0. \end{cases} \tag{20}$$

Due to the difference of mechanical responses of concrete in tension and compression, the damage variable is split into two parts

$$D = \alpha_t D_t + \alpha_c D_c, \tag{21}$$

where D_t and D_c are the damage variables in tension and compression, respectively. They are combined with the weighting coefficients α_t and α_c , defined as functions of the principal values of the strains ϵ_{t_i} and ϵ_{c_i} due to positive and negative stresses

$$\epsilon_t = (1 - D)C^{-1}\sigma_t, \quad \epsilon_c = (1 - D)C^{-1}\sigma_c. \tag{22}$$

The weights α_t and α_c are defined by the following expressions:

$$\alpha_t = \sum_{i=1}^3 \left(\frac{\langle \epsilon_{t_i} \rangle \langle \epsilon_{t_i} \rangle}{\tilde{\epsilon}^2} \right)^\beta, \quad \alpha_c = \sum_{i=1}^3 \left(\frac{\langle \epsilon_{c_i} \rangle \langle \epsilon_{c_i} \rangle}{\tilde{\epsilon}^2} \right)^\beta. \tag{23}$$

In uniaxial tension $\alpha_t = 1$ and $\alpha_c = 0$. In uniaxial compression $\alpha_c = 1$ and $\alpha_t = 0$. Hence, D_t and D_c can be obtained separately from uniaxial tests.

The evolution of damage is provided in an integrated form, as function of the variable κ

$$\begin{aligned} D_t &= 1 - \frac{\kappa_0(1 - A_t)}{\kappa} - \frac{A_t}{\exp[B_t(\kappa - \kappa_0)]}, \\ D_c &= 1 - \frac{\kappa_0(1 - A_c)}{\kappa} - \frac{A_c}{\exp[B_c(\kappa - \kappa_0)]}. \end{aligned} \tag{24}$$

4.1.3. Identification of parameters

There are eight model parameters. Young’s modulus and Poisson’s ratio are measured from a uniaxial compression test. A direct tensile test or three-point bend test can provide the damage parameters in tension (κ_0 , A_t , B_t). The parameters (A_c , B_c) are fitted from the response of the material to uniaxial compression. Finally, β should be fitted from the response of the material to shear and usually its value is $\beta = 1$. Table 5 presents the standard intervals for the model parameters in the case of concrete [49].

4.1.4. Numerical example

In this example the isotropic damage model is implemented in the finite element code FEAP. This material model is only applied to the mortar matrix whereas the aggregates are assumed to behave linearly elastic. Fig. 12(a) shows the geometrical configuration of the aggregates within the specimen.

Table 5
Standard model parameters

Parameters of isotropic damage model
$\kappa_0 \approx 1 \times 10^{-4}$
$0.7 \leq A_t \leq 1.2$
$10^4 \leq B_t \leq 5 \times 10^4$
$1 \leq A_c \leq 1.5$
$10^3 \leq B_c \leq 2 \times 10^3$
$1.0 \leq \beta \leq 1.05$

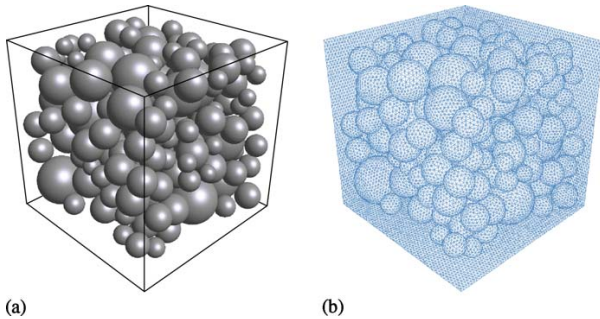


Fig. 12. Concrete specimen. (a) Geometrical configuration ($v_p=40\%$ and 181 particles). (b) Finite element mesh (139 902 nodes and 773 405 elements).

Table 6
Material parameters of constituents

Mortar	Aggregates
$E = 20\,000 \text{ N/mm}^2$	$E = 60\,000 \text{ N/mm}^2$
$\nu = 0.20$	$\nu = 0.22$
$\kappa_0 = 1.0 \times 10^{-4}$	–
$A_t = 1.2$	–
$B_t = 1.5 \times 10^4$	–
$A_c = 1.0$	–
$B_c = 1.555 \times 10^3$	–
$\beta = 1.0$	–

In this model only 40% of aggregate volume fraction is used in order to reduce the number of degrees of freedom (see Fig. 12(b)). In order to evaluate the validity of the numerical modelling, the results obtained from the finite element computations are compared with the experimental results of Cordes [60]. In Table 6 are given the material parameters of the concrete constituents used in the computations. The compressive loading is controlled by displacement to simulate the nonlinear material response of concrete in the softening regime.

Fig. 13 shows the stress–strain behaviour and damage evolution response of the simulated uniaxial compression test as well as the experimental data under compressive loading. It can be seen in Fig. 13 that the numerically predicted response of $\epsilon - \sigma$ is in reasonably good accordance with the experimental results introduced in Cordes [60]. However, the numerical model overestimates the mechanical behaviour of concrete in the prepeak region. This disagreement might possibly be due to the fact that the ITZs have not been included in the numerical model. Experimental studies have shown that the ITZ has

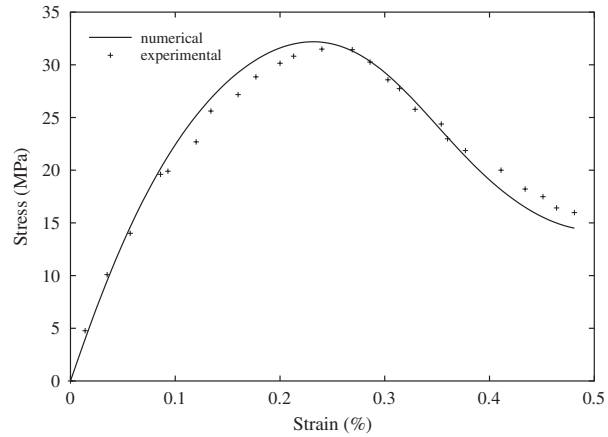


Fig. 13. Stress–strain behaviour under uniaxial compression.

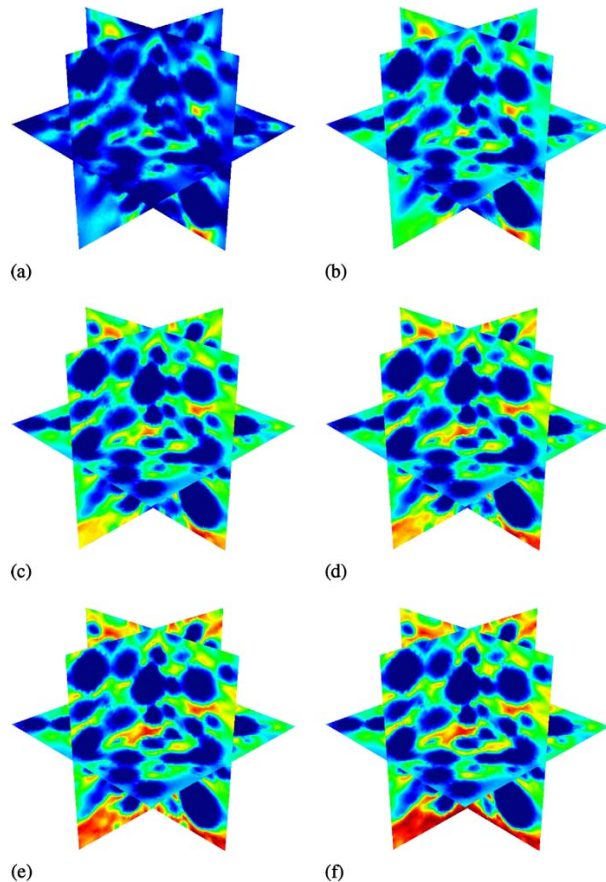


Fig. 14. Distribution of the damage parameter D . (a) $u_{33} = 32.90 \mu\text{m}$; (b) $u_{33} = 54.83 \mu\text{m}$; (c) $u_{33} = 120.63 \mu\text{m}$; (d) $u_{33} = 142.57 \mu\text{m}$; (e) $u_{33} = 175.47 \mu\text{m}$ and (f) $u_{33} = 230.30 \mu\text{m}$.

a significant effect on the bulk characteristics of concrete and, therefore, must be considered as a separate phase in the mechanical analysis of concrete.

It is also to be noted in the lower half of the softening regime that the mechanical response predicted by the numerical model tends to be slightly more brittle than in the experimental result. Such a disparity might be due to the strain localisation which is usually inherent to the local formulation of the isotropic damage model. Thus, nonlocal damage approaches should be used in future computations in order to limit strain localisation and to circumvent mesh sensitivity associated with strain softening.

The distribution of the damage parameter at several loading steps is shown in Fig. 14. It can be seen that the damage occurs in the mortar material around the aggregate particles. The coalescence of the damaged areas, which finally results in the failure of the material, is also to be clearly observed within the mortar matrix.

5. Conclusions

In this work the random aggregate structure of the concrete material at the mesoscopic level is generated. A new algorithm for generating realistic concrete models of high aggregate volume fractions is proposed. In this algorithm the intersecting particles are translated and then randomly rotated until a free position satisfying the placing requirements is found. The proposed algorithm shows that fast and good results can be obtained in generating numerical concrete models comparable to the ones in real concrete. In the case of high volume fractions of aggregate particles, there usually occur some difficulties in placing all the generated particles into the concrete volume. Therefore, a re-generation algorithm of the remaining particles is adopted.

The generated mesostructure models are then meshed using the aligned approach in which the finite element boundaries are coincident with materials interfaces and therefore there are no material discontinuities within the elements.

In the direct computation of the concrete effective properties the FEM is used. The results obtained from the numerical simulations are then compared with experimental data found in the literature. In general, the results of the finite element computations show a good agreement to the experimental data. Three-dimensional simulations of the aggregate shapes will be also unavoidable to study their effects on the effective elastic parameters of concrete.

In the numerical simulations of the damage and fracture process of concrete an isotropic damage model is applied in the numerical simulation of the mechanical behaviour of concrete under uniaxial compressive loading. In general, the numerically predicted response shows reasonably a good agreement with the experimental data. Nevertheless, interface elements with nonlinear material behaviour have to be included in the numerical model between the mortar and the aggregates to simulate the effect of the ITZ on the overall behaviour of concrete, see e.g. [61]. In addition, nonlocal damage formulations should be used in future work to cope with mesh sensitivity problems associated with strain softening.

References

- [1] Z.P. Bazant, M.R. Tabbara, M.T. Kazemi, G. Pijaudier-Cabot, Random particle model for fracture of aggregate or fiber composites, *J. Engng. Mech.* 116 (8) (1990) 1686–1705.
- [2] H. Schorn, U. Rode, Numerical simulation of crack propagation from microcracking to fracture, *Cem. Concr. Compos.* 13 (2) (1991) 87–94.
- [3] E. Schlangen, J.G.M. van Mier, Simple lattice model for numerical simulation of fracture of concrete materials and structures, *Mater. Struct.* 25 (153) (1992) 534–542.
- [4] H. Sadouki, F.H. Wittmann, On the analysis of the failure process in composite materials by numerical simulation, *Mater. Sci. Engng.* 104 (1988) 9–20.
- [5] F.H. Wittmann, P.E. Roelfstra, H. Sadouki, Simulation and analysis of composite structures, *Mater. Sci. Engng.* 68 (2) (1984) 239–248.
- [6] F.H. Wittmann, H. Sadouki, T. Steiger, Experimental and numerical study of effective properties of composite materials, in: *Micromechanics of Concrete and Cementitious Composites*, Presses Polytechniques et Universitaires Romandes, Lausanne, 1993, pp. 59–82.
- [7] Z.M. Wang, A.K.H. Kwan, H.C. Chan, Mesoscopic study of concrete I: generation of random aggregate structure and finite element mesh, *Comput. Struct.* 70 (5) (1999) 533–544.
- [8] Y.B. Zaitsev, F.H. Wittmann, Simulation of crack propagation and failure of concrete, *Mater. Struct.* 14 (2) (1981) 357–365.
- [9] J.K. Beddow, T. Meloy, *Testing and characterization of powders and fine particles*, Heyden, London, 1980.
- [10] A. Guidoum, P. Navi, Numerical simulation of thermomechanical behaviour of concrete through a 3D granular cohesive model, in: *Micromechanics of Concrete and Cementitious Composites*, Presses Polytechniques et Universitaires Romandes, Lausanne, 1993, pp. 213–228.
- [11] S. Häfner, S. Eckardt, C. Könke, A geometrical inclusion-matrix model for the finite element analysis of concrete at multiple scales, in: *Proceedings of the 16th IKM 2003*, Weimar, 2003.
- [12] J.P.B. Leite, V. Slowik, H. Mihashi, Computer simulation of fracture processes of concrete using mesolevel models of lattice structures, *Cement Concrete Res.* 34 (6) (2004) 1025–1033.
- [13] T.I. Zohdi, Computational optimization of the vortex manufacturing of advanced materials, *Comput. Methods Appl. Mech. Engrg.* 190 (46–47) (2001) 6231–6256.
- [14] E.J. Garboczi, Three-dimensional mathematical analysis of particle shape using X-ray tomography and spherical harmonics: Application to aggregates used in concrete, *Cement Concrete Res.* 32 (10) (2002) 1621–1638.
- [15] E. Schlangen, Experimental and numerical analysis of fracture processes in concrete, PhD thesis, Technische Universiteit Delft, 1993.
- [16] J.G.M. van Mier, M.R.A. van Vliet, T.K. Wang, Fracture mechanisms in particle composites: statistical aspects in lattice type analysis, *Mech. Mater.* 34 (11) (2002) 705–724.
- [17] G. De Schutter, L. Taerwe, Random particle model for concrete based on Delaunay triangulation, *Mater. Struct.* 26 (156) (1993) 67–73.
- [18] J.G.M. van Mier, M.R.A. van Vliet, Influence of microstructure of concrete on size/scale effects in tensile fracture, *Eng. Fract. Mech.* 70 (16) (2003) 2281–2306.
- [19] P.A. Cundall, O.D.L. Strack, A discrete numerical model for granular assemblies, *Geotechnique* 29 (1) (1979) 47–65.
- [20] S. Eckardt, S. Häfner, C. Könke, Simulation of the fracture behaviour of concrete using continuum damage models at the mesoscale, in: *Proceedings of ECCOMAS 2004*, Jyväskylä, 2004.
- [21] C. Huet, An integrated approach of concrete micromechanics, in: *Micromechanics of Concrete and Cementitious Composites*, Presses Polytechniques et Universitaires Romandes, Lausanne, 1993, pp. 117–146.

- [22] A.K.H. Kwan, Z.M. Wang, H.C. Chan, Mesoscopic study of concrete II: nonlinear finite element analysis, *Comput. Struct.* 70 (5) (1999) 545–556.
- [23] T.I. Zohdi, P. Wriggers, Aspects of the computational testing of the mechanical properties of microheterogeneous material samples, *Int. J. Numer. Meth. Eng.* 50 (11) (2001) 2573–2599.
- [24] S. Löhnert, Computational homogenization of microheterogeneous materials at finite strains including damage, PhD thesis, Hannover, IBNM, 2004.
- [25] E.J. Garboczi, Computational materials science of cement-based materials, *Materials and Structures* 26 (158) (1993) 191–195.
- [26] H.M. Jennings, S.K. Johnson, Simulation of microstructure development during the hydration of a cement compound, *J. Am. Ceram. Soc.* 69 (11) (1986) 790–795.
- [27] Y. Xi, P.D. Tennis, H.M. Jennings, Mathematical modeling of cement paste microstructure by mosaic pattern: Part I Formulation, *J. Mater. Res.* 11 (8) (1996) 1943–1952.
- [28] D.P. Bentz, E.J. Garboczi, Guide to using HYDRA3D: A three-dimensional digital-image-based cement microstructural model, U.S. Department of Commerce, Gaithersburg, 1992. N.I.S.T. Internal Report 4746.
- [29] K. Terada, T. Miura, N. Kikuchi, Digital image-based modeling applied to the homogenization analysis of composite materials, *Computational Mechanics* 20 (1997) 331–346.
- [30] P.E. Roelfstra, A numerical approach to investigate the properties of concrete: numerical concrete, PhD thesis, Lausanne, EPFL, 1989.
- [31] T.J. Hirsch, Modulus of elasticity of concrete affected by elastic moduli of cement paste matrix and aggregate, *Journal Proceedings, ACI* 59 (1962) 427–452.
- [32] T.I. Zohdi, P. Wriggers, Computational micro-macro material testing, *Arch. Comp. Meth. Eng.* 8 (2) (2001) 131–228.
- [33] J. Aboudi, *Mechanics of Composite Materials: A Unified Micromechanical Approach*, Elsevier, Amsterdam, 1991.
- [34] R. Hill, Elastic properties of reinforced solids: some theoretical principles, *J. Mech. Phys. Solids* 11 (5) (1963) 357–372.
- [35] W. Voigt, Über die Beziehung zwischen den beiden Elastizitätskonstanten isotroper Körper, *Wied. Ann.* 38 (1889) 573–587.
- [36] A. Reuss, Berechnung der Fließgrenz von Mischkristallen auf Grund der Plastizitätsbedingung für Einkristalle, *Z. Angew. Math. Mech.* 9 (1929) 49–58.
- [37] R. Hill, The elastic behaviour of a crystalline aggregate, *Proc. Phys. Soc. (Lond.)*, A 65 (389) (1952) 349–355.
- [38] J.D. Eshelby, The elastic field of an ellipsoidal inclusion, and related problems, *Proc. Roy. Soc. A* 241 (1957) 376–396.
- [39] Z. Hashin, S. Shtrikman, On some variational principles in anisotropic and nonhomogeneous elasticity, *J. Mech. Phys. Solids* 10 (4) (1962) 335–342.
- [40] T. Mori, K. Tanaka, Average stress in matrix and average energy of materials with misfitting inclusions, *Acta. Metall.* 21 (5) (1973) 571–574.
- [41] R. Christensen, A critical evaluation for a class of micromechanics models, *J. Mech. Phys. Solids* 38 (3) (1990) 379–404.
- [42] T.I. Zohdi, P. Wriggers, *Introduction to Computational Micromechanics*, Springer, Berlin, 2005.
- [43] R.M. Christensen, *Mechanics of Composite Materials*, Wiley, New York, 1979.
- [44] Z. Hashin, Analysis of composite materials: a survey, *ASME Journal of Applied Mechanics* 50 (3) (1983) 481–505.
- [45] S. Nemat-Nasser, M. Hori, *Micromechanics: overall properties of heterogeneous solids*, Elsevier, Amsterdam, 1999.
- [46] Z. Hashin, S. Shtrikman, A variational approach to the theory of the elastic behaviour of multiphase materials, *J. Mech. Phys. Solids* 11 (2) (1963) 127–140.
- [47] A.F. Stock, D.J. Hannant, R.I.T. Williams, Effect of aggregate concentration upon the strength and modulus of elasticity of concrete, *Mag. Concrete Res.* 31 (109) (1979) 225–234.
- [48] A. Carpinteri, M.H. Aliabadi, *Computational Fracture Mechanics in Concrete Technology*, WIT Press, Southampton, 1999.
- [49] J. Lemaitre, *Handbook of Materials Behavior Models: Failures of Materials*, vol. 2, Academic Press, San Diego, 2001.
- [50] J. Lemaitre, J.P. Sermage, One damage law for different mechanisms, *Computational Mechanics* 20 (1997) 84–88.
- [51] P. Fanning, O. Kelly, Smear crack models of rc beams with externally bonded cfrp plates, *Computational Mechanics* 26 (2000) 325–332.
- [52] J.G. Rots, *Computational modeling of concrete fracture*. PhD thesis, Technische Universiteit Delft, 1988.
- [53] E. Schlangen, E.J. Garboczi, Fracture simulations of concrete using lattice models: computational aspects, *Eng. Fract. Mech.* 57 (2-3) (1997) 319–332.
- [54] G. Lilliu, J.G.M. van Mier, 3D lattice type fracture model for concrete, *Eng. Fract. Mech.* 70 (7–8) (2003) 927–941.
- [55] D. Krajcinovic, Distributed damage theory of beams in pure bending, *ASME Journal of Applied Mechanics* 46 (3) (1979) 592–596.
- [56] J. Mazars, G. Pijaudier-Cabot, Continuum damage theory - application to concrete, *J. Engrg. Mech. ASCE* 115 (2) (1987) 345–365.
- [57] J. Mazars, G. Pijaudier-Cabot, From damage to fracture mechanics and conversely: A combined approach, *Int. J. Solid. Struct.* 33 (20–22) (1996) 3327–3342.
- [58] R.H.J. Peerlings, *Enhanced damage modelling for fracture and fatigue*. PhD thesis, Technische Universiteit Eindhoven, 1999.
- [59] J. Mazars, A description of microscale and macroscale damage of concrete structures, *Eng. Fract. Mech.* 25 (5–6) (1986) 729–737.
- [60] H. Cordes, Über die Spannungs-Dehnungs-Linie von Beton bei kurzzeitiger Lasteinwirkung, PhD thesis, Technische Universität Hannover, 1968.
- [61] P. Wriggers, G. Zavarise, T. Zohdi, A computational study of interfacial debonding damage in fibrous composites materials, *Computational Materials Science* 12 (1998) 39–56.